Expanded View Figures

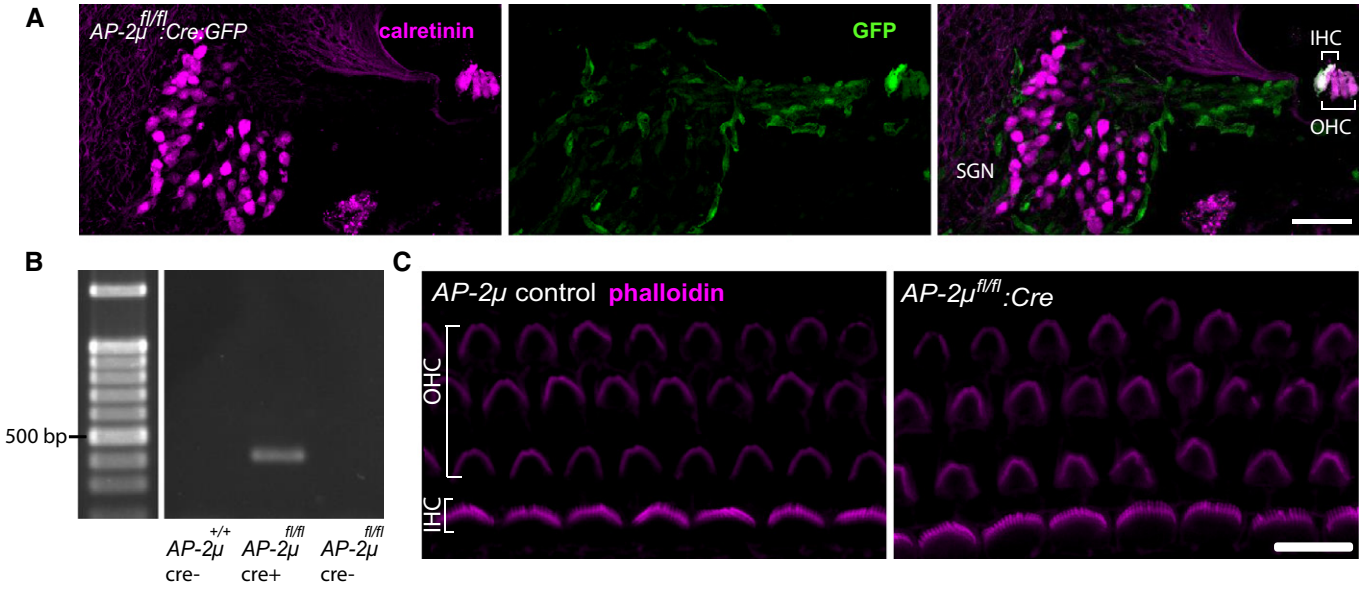

Figure EV1. Generation of hair cell-specific *AP-2μ* knockout mice (*AP-2μ$^{fl/fl}$:Cre*).

A Cryosectioned cochlea of a p7 *AP-2μ$^{fl/fl}$:Cre* mouse demonstrates VGLUT3-driven Cre recombination in IHCs and OHCs (Jung *et al*, 2015) but not in SGNs, as reported by a floxed EGFP reporter (Nakamura *et al*, 2006). Immunohistochemical staining for calretinin (magenta), marking IHCs, OHCs, and SGNs and native EGFP fluorescence (green), indicating Cre recombination. In addition to EGFP signal in hair cells, some EGFP expression was found in capillaries and supporting cells. Scale bar, 50 μm.

B PCR of genomic DNA extracted from microdissected cochlea of p21 mice shows amplification of the Cre-recombined region in Cre-expressing *AP-2μ$^{fl/fl}$* mice ((Kononenko *et al*, 2014), middle column), but not in *AP-2μ* control: C57Bl/6 expressing Cre (left column) or *AP-2μ$^{fl/fl}$* mice lacking Cre (right column). Genomic DNA was isolated from whole cochleae of *AP-2μ$^{fl/fl}$:Cre:GFP*, *AP-2μ$^{fl/fl}$*, and *AP-2μ$^{+/+}$:Cre* mice with the nexttec™ kit (nexttec Biotechnologie GmbH, Germany). PCR was performed using DreamTaq DNA polymerase (Fermentas). The Cre-recombinated excision of exon 2–3 in the *Ap-2μ* gene was confirmed by using the forward primer TM330 GCTCTAAAGGTTATGCCTGGTGG and the reverse primer TM191 CCAAGGGACCTACAGGACTTC that detected a fragment of 404 bp (PCR at 58°C, 25 cycles) in cochlear DNA.

C Phalloidin immunofluorescence shows apparently intact stereociliar bundles (magenta) of IHCs (1 row) and OHCs (three rows) in acutely dissected apical coils of the cochlea from *AP-2μ$^{fl/fl}$* control and *AP-2μ$^{fl/fl}$:Cre* mice at p7. Scale bar, 10 μm.

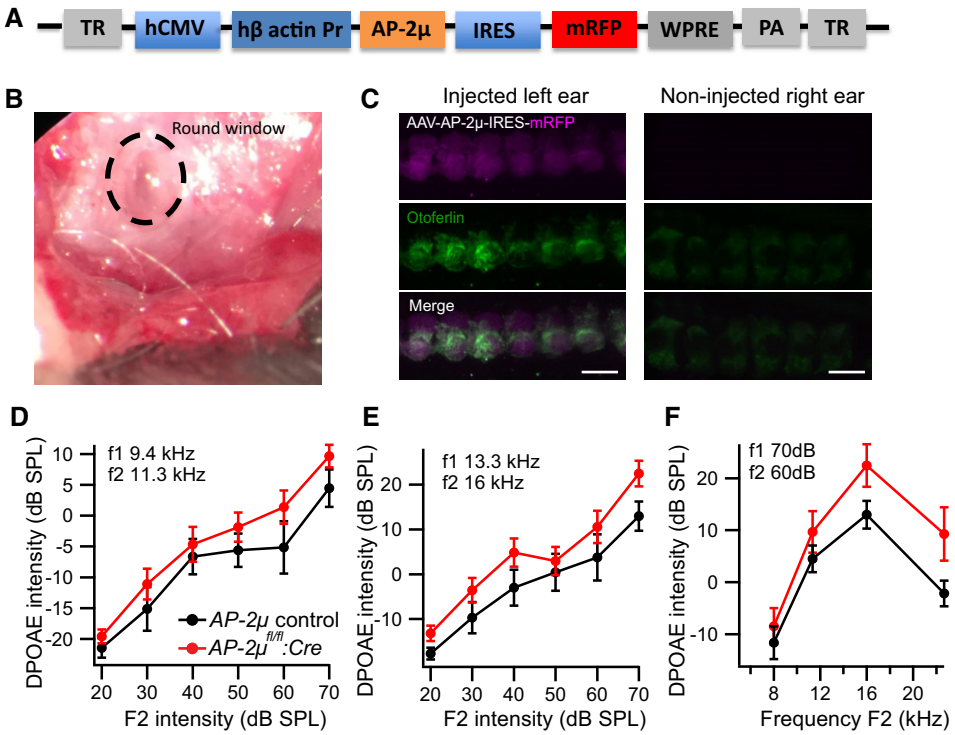

Figure EV2. Viral rescue of AP-2μ expression in *AP-2μ$^{fl/fl}$:Cre:GFP* mice and intact cochlear amplification by OHCs in *AP-2μ$^{fl/fl}$:Cre:GFP* mice.

A Illustration of the vector for AAV2/1-mediated rescue of hearing in *AP-2μ$^{fl/fl}$:Cre:GFP* mice. *AP-2μ* is expressed under the CMV-enhanced human β-actin promoter, and mRFP was used as a reporter gene under the control of the internal ribosome entry site (IRES).

B Surgical situs for AAV injection into the scala tympani of the left ear. In brief, a retroauricular incision was made, skin, connective tissue, and musculature retracted by a custom stainless steel retractor, and the bulla opened carefully with fine forceps to just expose the round window niche. A 10- to 20-μm tip glass pipette was filled with AAV suspension and fast green dye and used to inject 2–3 shots of virus suspension (0.2–0.5 μl of 4.32E12 genome copies/ml, packaged at Penn Vector Core) at 0.13–0.34 bar using a pico-injector (PL1–100, Harvard Apparatus). The wound was closed with adipose tissue and mice recovered and finally returned to the dam. This procedure led to no or minimal ABR threshold increases when injecting wild-type ears with AAV carrying either fluorescent protein or AP-2μ along with the fluorescent protein (data not shown).

C Transduction of *AP-2μ$^{fl/fl}$:Cre:GFP* IHCs via postnatal injection of AAV-AP-2μ-mRFP into the cochlear perilymph of the left ear on postnatal day 10 as indicated by native mRFP fluorescence (magenta) in otoferlin (green)-immunolabeled IHCs. In contrast, there was no mRFP signal and much less otoferlin immunofluorescence in the non-injected right ear of the same mouse. Scale bar, 10 μm.

D, E Average DPOAE growth functions in response to pairs of primary tones of 9.4 kHz and 11.3 kHz (B) or 13.3 kHz and 16 kHz (C) at varying intensities ± SEM for *AP-2μ$^{fl/fl}$:Cre:GFP* (red, n = 11) and *AP-2μ* control (black, n = 8).

F Average DPOAE-Grams in response to pairs of primary tones with varying frequencies (f2 = 1.2 × f1) ± SEM for *AP-2μ$^{fl/fl}$:Cre:GFP* (red, n = 11) and *AP-2μ* control (black, n = 8).

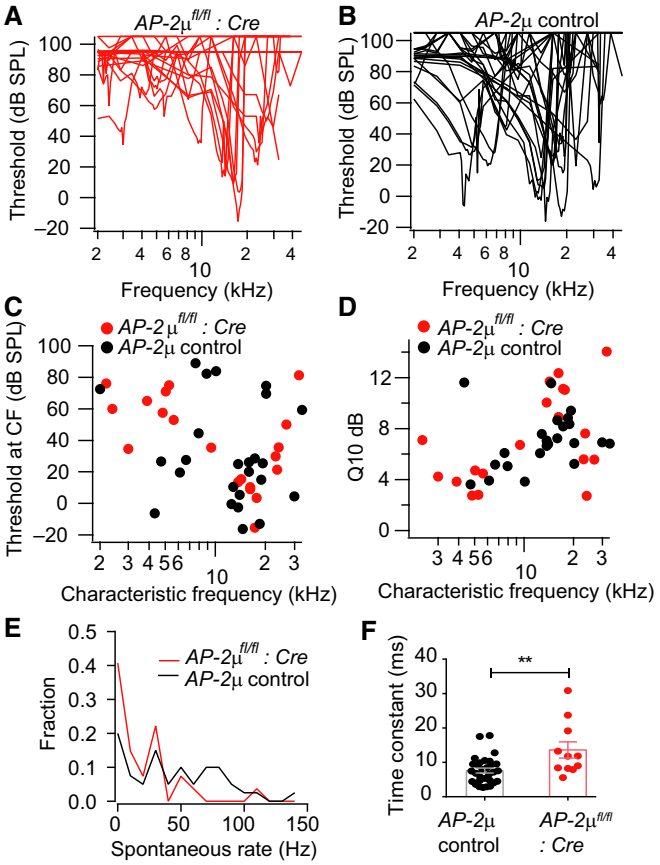

Figure EV3. Frequency tuning, sound threshold, spontaneous firing, kinetics, and extent of short-term adaptation in SGNs of *AP-2μ*$^{fl/fl}$*:Cre:GFP* mice.

A, B Frequency tuning curves of SGNs in *AP-2μ*$^{fl/fl}$*:Cre:GFP* mice (A) show comparable thresholds and sharpness of tuning as in SGN of *AP-2μ* control mice (B), compatible with normal cochlear function upstream of the IHC synapse (Fig EV2D–F).

C Sound thresholds at the characteristic frequency of putative SGNs in *AP-2μ*$^{fl/fl}$*:Cre:GFP* mice were comparable to those of SGNs of *AP-2μ* control mice.

D Frequency tuning, quantified as the excitatory bandwidth at 10 dB above threshold divided by the frequency (Q10 dB), was comparable between *AP-2μ*$^{fl/fl}$*:Cre:GFP* mice and *AP-2μ* control mice.

E Spontaneous rate distributions of *AP-2μ*$^{fl/fl}$*:Cre:GFP* (n = 27) and *AP-2μ* control (n = 40) SGNs differ significantly (P = 0.011, Kolmogorov–Smirnov) with lower rates in *AP-2μ*$^{fl/fl}$*:Cre:GFP* mice.

F Slower kinetics of short-term spike rate adaptation ($P < 0.01$, Wilcoxon rank-sum test), indicating a reduced replenishment and/or fusion rate constant of the RRP.

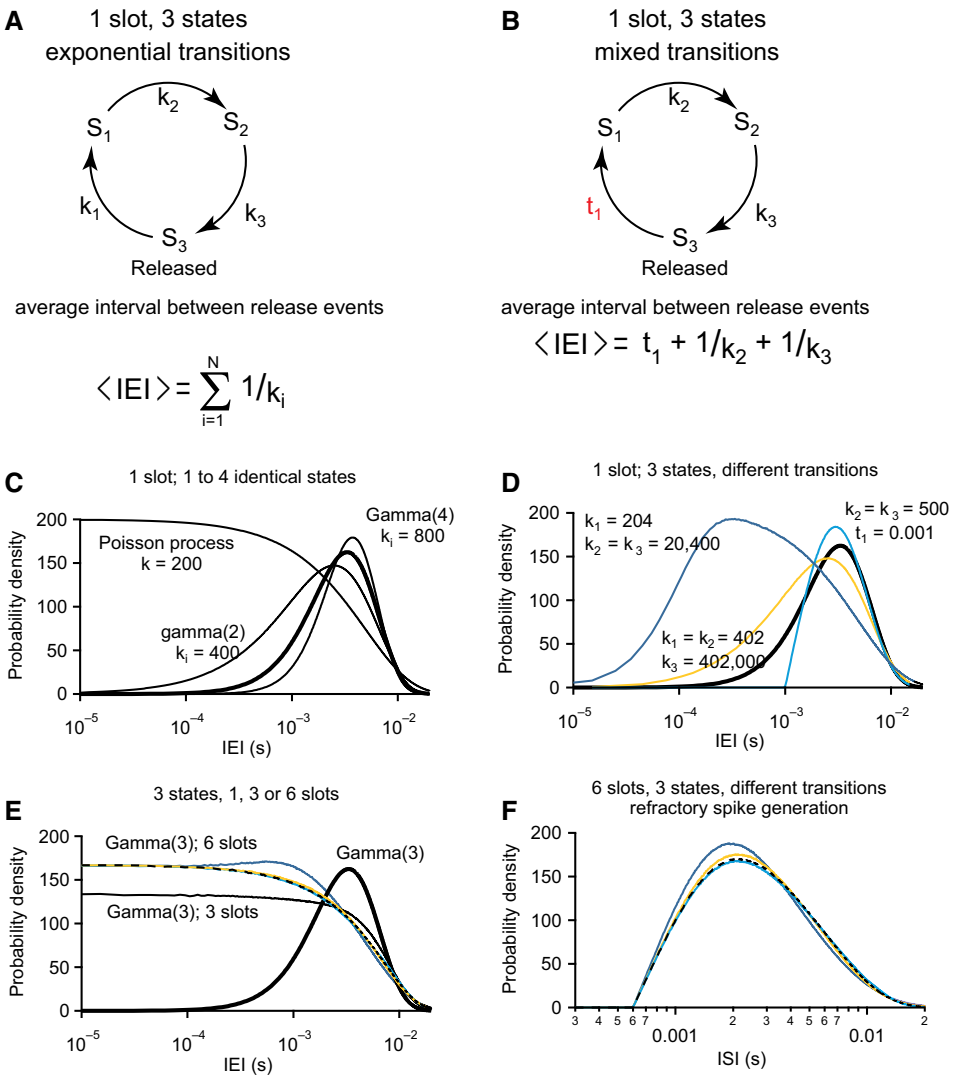

Figure EV4. Details of the pre-synaptic release site kinetics are reflected in release and spike statistics.

A Model of the vesicle release/refill cycle at a single release site ("slot") based on a Markov model with *N* states, in this example *N* = 3. The transitions into state i occurs as Poisson process with rate k_i. If all *N* rates are identical, the intervals between release events follow a gamma distribution with form factor *N* (see C).

B One of the Poisson transitions is replaced by a transition that takes a fixed time, as it would occur when active clearance was replaced by clearance through diffusion.

C The probability density function of IEIs for release site models with 1–4 states and identical transitions. The rate constants are given in s^{-1}. For three states (thick line), k_i = 600/s. The memoryless Poisson process (*N* = 1) contributes much more very short IEIs. The transition rates were adapted to obtain an average release rate of 200/s in all cases.

D The IEI distribution of a three-state-cycle with identical transitions follows a gamma distribution with form factor 3 (thick line). If the first one of the transitions becomes much faster, the IEI distribution shifts toward gamma with form factor 2 (orange), if also a second transition becomes faster, the single remaining slow transition is speed limiting and the IEI distribution shifts toward a Poisson distribution (dark blue). When one of the transitions is replaced by a fixed waiting time t_1, the IEI distribution shifts in the other direction (cyan). As no intervals shorter than t_1 are now possible, the probability density concentrates toward longer intervals.

E As release events from more than one release site are combined, very short IEIs can occur and the result resembles a mixture of a Poisson process and a gamma process (thin continuous black line: three states, dashed line six states) even if each individual release site produces gamma(3)-distributed events. This blurs the clear differences observed for a single release site (compare to D, corresponding simulations in identical color code). Data are generated with the same relative rate differences as in (C), but all rates are scaled to obtain an average release rate of 200/s from the one, three or six release sites combined.

F The refractory spike generation further transforms the probability density functions. Intervals below the absolute refractory period no longer occur, and the distributions are deformed toward longer intervals.

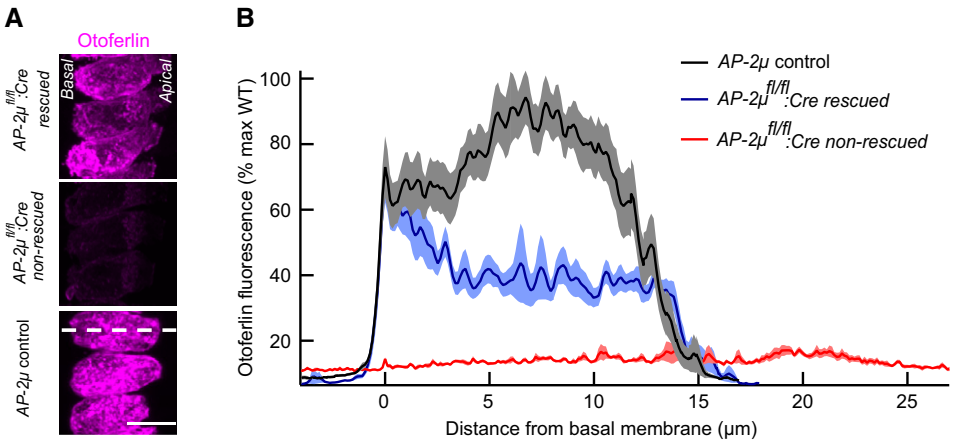

Figure EV5. AAV2/1 gene replacement of AP-2μ restores near-normal otoferlin protein levels in IHCs of *AP-2μ$^{fl/fl}$:Cre* mouse.

A Maximum projections of confocal sections of otoferlin-immunolabeled organs of Corti of p14–17 *AP-2μ$^{fl/fl}$:Cre* rescued (AAV-AP-2μ-injected; upper panel), *AP-2μ$^{fl/fl}$:Cre* non-rescued (middle panel), and *AP-2μ* control (bottom panel) ears that were stained and imaged in parallel under identical conditions. Scale bar, 10 μm.

B Average line profiles along the long axis of the IHCs (white dotted line in the bottom panel of A) reveal an increased otoferlin immunofluorescence in rescued IHCs, in particular at the plasma membrane in the basal pole where normal protein levels are found. Data were normalized to maximum fluorescence of IHCs from *AP-2μ* control ears, originate from n = 19 IHCs for *AP-2μ* control, n = 12 IHCs for *AP-2μ$^{fl/fl}$:Cre* rescued, and n = 7 IHCs for *AP-2μ$^{fl/fl}$:Cre* non-rescued and are presented as mean ± SEM. The basal pole of the IHCs points to the left in the images. IHCs from *AP-2μ$^{fl/fl}$:Cre* rescued and *AP-2μ* control ears happened to extend at a steeper angle within the organ of Corti in this sample than usual, giving rise to the shorter profiles in the maximum projection.